



1 **Large contribution of fossil-fuel derived secondary organic**
2 **carbon to water-soluble organic aerosols in winter haze of China**

3 Yan-Lin Zhang^{1,2,3*}, Imad El-Haddad³, Ru-Jin Huang^{3,4*}, Kin-Fai Ho^{4,5}, Jun-Ji Cao^{4*},
4 Yongming Han⁴, Peter Zotter^{3,#}, Carlo Bozzetti³, Kaspar R. Daellenbach³, Jay G. Slowik³, Gary
5 Salazar², André S.H. Prévôt^{3*}, Sönke Szidat^{2*}

6 ¹Yale-NUIST Center on Atmospheric Environment, Nanjing University of Information Science
7 and Technology, 210044 Nanjing, China

8 ²Department of Chemistry and Biochemistry & Oeschger Centre for Climate Change Research,
9 University of Bern, 3012 Bern, Switzerland

10 ³Paul Scherrer Institute (PSI), 5232 Villigen, Switzerland

11 ⁴Key Laboratory of Aerosol Chemistry and Physics, Institute of Earth Environment, Chinese
12 Academy of Sciences, 710061 Xi'an, China

13 ⁵School of Public Health and Primary Care, The Chinese University of Hong Kong, Hong Kong,
14 China

15 *To whom correspondence should be addressed. E-mail: dryanlinzhang@outlook.com or
16 zhangyanlin@nuist.edu.cn (Y.-L.Z.); andre.prevot@psi.ch (A. Prévôt); rujin.huang@ieecas.cn
17 (R.-J.H.); jjcao@ieecas.cn (J.J.C.); szidat@deb.unibe.ch (S.S.).

18 Phone: +86 25 5873 1022; fax: +86 25 5873 1193



19 **Abstract**

20 Water-soluble organic carbon (WSOC) is a large fraction of organic aerosols (OA) globally and
21 has significant impacts on climate and human health. The sources of WSOC remain very
22 uncertain in polluted regions. Here we present a quantitative source apportionment of WSOC
23 isolated from aerosols in China using radiocarbon (^{14}C) and offline high-resolution time-of-
24 flight aerosol mass spectrometer measurements. Fossil emissions on average accounted for 32-
25 47% of WSOC. Secondary organic carbon (SOC) dominated both the non-fossil and fossil
26 derived WSOC, highlighting the importance of secondary formation to WSOC in severe winter
27 haze episodes. Contributions from fossil emissions to SOC were $61\pm 4\%$ and $50\pm 9\%$ in
28 Shanghai and Beijing, respectively, significantly larger than those in Guangzhou ($36\pm 9\%$) and
29 Xi'an ($26\pm 9\%$). The most important primary sources were biomass burning emissions,
30 contributing 17-26% of WSOC. The remaining primary sources such as coal combustion,
31 cooking and traffic were generally very small but not negligible contributors, as coal
32 combustion contribution could exceed 10%. Taken together with earlier ^{14}C source
33 apportionment studies in urban, rural, semi-urban, and background regions in Asia, Europe and
34 USA, we demonstrated a dominant contribution of non-fossil emissions (i.e., $75\pm 11\%$) to
35 WSOC aerosols in the North Hemisphere; however, the fossil fraction is substantially larger in
36 aerosols from East Asia and the East Asian pollution outflow especially during winter due to
37 increasing coal combustion. Inclusion of our findings can improve a modelling of effects of
38 WSOC aerosols on climate, atmospheric chemistry and public health.



39 1 INTRODUCTION

40 Water-soluble organic carbon (WSOC) is a large fraction of atmospheric organic
41 aerosols (OA), which contributes approximately 10% to 80% of the total mass of organic carbon
42 (OC) in aerosols from urban, rural and remote sites (Zappoli et al., 1999;Weber et al.,
43 2007;Ruellan and Cachier, 2001;Wozniak et al., 2012;Mayol-Bracero et al., 2002). Only 10 to
44 20% of total mass of WSOC has been resolved at a molecular level, and it consists of a large
45 variety of chemical species such as mono- and di-carboxylic acids, carbohydrate derivatives,
46 alcohols, aliphatic and aromatic acids and amino acids (Fu et al., 2015;Noziere et al., 2015).
47 Recent studies suggest that the water-soluble fraction of HUMic LIke Substances (HULIS) is
48 a major component of WSOC, which exhibits light-absorbing properties (Limbeck et al.,
49 2005;Andreae and Gelencser, 2006;Laskin et al., 2015). Therefore, WSOC has significant
50 influences on the Earth's climate either directly by scattering and absorbing radiation or
51 indirectly by altering the hygroscopic properties of aerosols and increasing cloud condensation
52 nuclei (CCN) activity (Asa-Awuku et al., 2011;Cheng et al., 2011;Hecobian et al., 2010).

53 WSOC can be directly emitted as primary particles mainly from biomass burning
54 emissions or produced from secondary organic aerosol (SOA) formation (Sannigrahi et al.,
55 2006;Kondo et al., 2007;Weber et al., 2007;Bozzetti et al., 2017b;Bozzetti et al., 2017a).
56 Ambient studies provide evidence that SOA formation through the oxidation of volatile organic
57 compounds (VOCs) and gas-to-particle conversion processes may be a prevalent source of
58 WSOC (Kondo et al., 2007;Weber et al., 2007;Miyazaki et al., 2006;Hecobian et al., 2010).
59 WSOC is therefore thought to be a good proxy of secondary organic carbon (SOC) in the
60 absence of biomass burning (Weber et al., 2007). By contrast, water-insoluble OC (WIOC) is
61 thought to be mainly from primary origins with a substantial contribution from fossil fuel
62 emissions (Miyazaki et al., 2006;Zhang et al., 2014b).

63 Due to a large variety of sources and unresolved formation processes of WSOC, their
64 relative fossil and non-fossil contributions are still poorly constrained. Radiocarbon (^{14}C)
65 analysis of sub-fractions of organic aerosols such as OC, WIOC and WSOC enable an



66 unambiguous, precise and quantitative determination of their fossil and non-fossil sources
67 (Zhang et al., 2012;Zhang et al., 2014b;Zhang et al., 2014c). Meanwhile, the application of
68 aerosol mass spectrometer measurement and positive matrix factorization and multi-linear
69 engine 2 (ME-2) can quantitatively classify organic aerosols into two major types such as
70 hydrocarbon-like OA (HOA) from primary fossil-fuel combustion and oxygenated organic
71 aerosol (OOA) from secondary origin (Zhang et al., 2007;Jimenez et al., 2009). Field
72 campaigns with the aerosol mass spectrometer (AMS) have revealed a predominance of OOA
73 in various atmospheric environments, although their sources remain poorly characterized
74 (Zhang et al., 2007;Jimenez et al., 2009). Previous studies found OOA is strongly correlated
75 with WSOC from urban aerosols in Tokyo, Japan, the Pearl River Delta (PRD) in South China
76 and Helsinki, Finland, indicating similar chemical characteristics, sources and formation
77 processes of OOA and WSOC (Kondo et al., 2007;Xiao et al., 2011;Timonen et al., 2013).
78 Similarly, HOA is mostly water insoluble and the major portion of water insoluble OC (WIOC)
79 can be assigned as HOA (Kondo et al., 2007;Daellenbach et al., 2016). Therefore, ^{14}C
80 measurement of WIOC and WSOC aerosols may provide new insights into sources and
81 formation processes of primary and secondary OA, respectively, which also will elucidate the
82 origin of HOA and OOA as measured by AMS (Zotter et al., 2014b).

83 In this paper we apply a newly developed method to measure ^{14}C in WSOC of $\text{PM}_{2.5}$
84 (particulate matter with an aerodynamic diameter of small than $2.5\ \mu\text{m}$) samples collected at
85 four Chinese megacities during an extremely severe haze episode during winter 2013 (Zhang
86 et al., 2015;Huang et al., 2014). In conjunction with our previous dataset from the same
87 campaign, we quantify fossil and non-fossil emissions from primary and secondary sources of
88 WSOC and WIOC. The dataset is also complemented by previous ^{14}C -based source
89 apportionment studies conducted in urban, rural and remote regions in the North Hemisphere
90 to gain an overall picture of the sources of WSOC aerosols.

91 2 MATERIALS AND METHODS



92 2.1 Sampling

93 During January 2013 extremely high concentrations of 24-h $PM_{2.5}$ (i.e. often >100
94 $\mu\text{g}/\text{m}^3$) were identified in several large cities in East China (Huang et al., 2014; Zhang et al.,
95 2015). To investigate sources and formation mechanisms of the haze particles, an intensive
96 field campaign was carried out in four large cities, Beijing, Xi'an, Shanghai and Guangzhou,
97 which are representative cities of the Beijing-Tianjin-Hebei region, central-northwest region,
98 Yangtze Delta Region, and Pearl River Delta Region, respectively. The sampling procedures
99 have been previously described in detail elsewhere (Zhang et al., 2015). Briefly, $PM_{2.5}$ samples
100 were collected on pre-baked (450 °C for 6 hours) quartz filters using high-volume samplers for
101 24 h at a flow rate of $\sim 1.05 \text{ m}^3/\text{min}$ from 5 to 25 January 2013. The sampling sites in each city
102 were located at campuses of universities or at research institutes, at least 100 m away from
103 major emission sources (e.g., roadways, industry and domestic sources). One field blank sample
104 for each site was collected and analyzed. The results reported here were corrected for these field
105 blanks (Zotter et al., 2014a; Cao et al., 2013). All samples were stored at -20 °C before analysis.
106 The $PM_{2.5}$ mass was gravimetrically measured with an analytical microbalance before and after
107 sampling with the same conditions (~ 12 hour)

108 2.2 OC and EC mass determinations

109 A 1.0 cm^2 filter punches were used for OC and EC mass determination with a OC/EC
110 analyzer (Model4L) using the EUSAAR_2 protocol (Cavalli et al., 2010). The replicate analysis
111 ($n=6$) showed an analytical precision with relative standard deviations smaller than 5%, 10%,
112 and 5% for OC, EC and TC, respectively. The field blank of OC was on average 2.0 ± 1.0
113 $\mu\text{g}/\text{cm}^2$ (equivalent to $\sim 0.5 \mu\text{g}/\text{m}^3$), which was used for blank correction for OC. EC data was
114 not corrected for field blank, because such a blank was not detectable.

115 2.3 Offline-AMS measurement and PMF source apportionment

116 The water-soluble extracts from the same samples were analyzed by a high resolution time of
117 flight aerosol mass spectrometer (HR-ToF-AMS) and the resulting mass spectra were used as



118 an inputs for positive matrix factorization (PMF) for the source apportionment of the WSOC,
119 OC and PM_{2.5}. The methodology applied, and the AMS-PMF results obtained are detailed in
120 Huang et al. (2014) and will only be briefly described in the following.

121 Filter punches (the equivalent of ~4 cm²) were sonicated in 10 mL ultrapure water (18.2 MΩ
122 cm at 25 °C, TOC <3ppb) for 20 min at 30°C. The water extracts were aerosolized and the
123 resulting particles were dried with a silica gel diffusion dryer before analysis by the HR-ToF-
124 AMS. For each measurement ten mass spectra were recorded (AMS V-mode, m/z 12-500), with
125 a collection time for each spectrum of 1 minute.

126 Online AMS measurements provide quantitative mass spectra of submicron non-refractory
127 aerosol species, including organic aerosol and ammonium nitrate and sulfate. However, the
128 offline AMS measurements described herein cannot be directly related to ambient
129 concentrations due to uncertainties in filter extraction and nebulization. In Huang et al. (2014),
130 the obtained mass spectra were scaled to the organic aerosol mass, obtained from the organic
131 carbon concentrations from the Sunset analyzer times the OM/OC ratios determined by the
132 AMS. Since the AMS-measured species are not extracted and aerosolized with equal efficiency,
133 PMF outputs were corrected using factor dependent recoveries. Here, this correction, which is
134 the main source of uncertainties reported in Huang et al. (2014), was not required any more
135 since here only WSOC PMF is present and organic aerosol mass spectra are directly scaled to
136 water soluble organic aerosol concentrations (WSOM, obtained as WSOC times OM/OC ratios).

137 The quantitative WSOM mass spectra are used together with other aerosol species (listed
138 below), collectively referred to as ‘species’ hereafter, as PMF inputs. PMF solves the bilinear
139 matrix equation:

$$140 \quad X_{ij} = \sum_k G_{i,k} F_{k,j} + E_{i,j} \quad (\text{Eq. 1})$$

141 by following the weighted least squares approach. In the equation, *i* represent the time index, *j*
142 a species and *k* the factor number. *X_{ij}* is the input matrix and *s_{ij}* the corresponding error matrix.
143 *G_{i,k}* is the matrix of the factor time-series, *F_{k,j}* is the matrix of the factor profiles and *E_{i,j}* the



144 model residual matrix. PMF determines $G_{i,k}$ and $F_{k,j}$ such that the ratio of the Frobenius norm
145 of $E_{i,j}$ over $s_{i,j}$ is minimised.

146 The species considered as inputs include the quantitative WSOM mass spectra, organic markers
147 (3 anhydrous sugars, 4 lignin breakdown products, 2 resin acids, 4 hopanes, 19 polycyclic
148 aromatic hydrocarbons and their oxygenated derivatives), EC, and major ions (Cl^- , NO_3^- , SO_4^{2-} ,
149 oxalate, methylsulfonic acid, Na^+ , K^+ , Mg^{2+} , Ca^{2+} , and NH_4^+) and residual PM. The latter is the
150 difference between total $\text{PM}_{2.5}$ mass and the measured species. It represents our best estimate
151 of the particulate chemical species not measured here, most likely dominated by crustal material.

152 The Source Finder toolkit (SoFi v.4.9) (Canonaco et al., 2013) for IGOR Pro software package
153 (Wavemetrics, Inc., Portland, OR, USA) was used to run the PMF algorithm. The PMF was
154 solved by the Multilinear Engine 2 (ME-2, Paatero, 1999), which allows the constraining of the
155 $F_{k,j}$ elements to vary within a certain range defined by the scalar α ($0 \leq \alpha \leq 1$), such that the
156 modelled $F'_{k,j}$ equals:

$$157 \quad F'_{k,j} = F_{k,j} \pm \alpha * F_{k,j} \quad (\text{Eq. 2})$$

158 The elements that were constrained in $F_{k,j}$ matrix can be found in Huang et al. (2014). The
159 factors extracted by ME-2 were interpreted to be related to primary emissions from traffic (TR),
160 biomass burning (BB), coal burning (CC), cooking emissions (CI) and dust and from two
161 secondary aerosol fractions. The contribution of the water soluble organic aerosol related to
162 these different factors are extracted and divided by the respective OM/OC_k calculated from the
163 high-resolution analysis of the factor mass spectral profile, to obtain the WSOC_k time series
164 related to each of the factors. In the following analysis, the mass of WSOC_k related to coal
165 burning and traffic were assigned to fossil WSOC fraction, while the mass of WSOC_k related
166 to biomass burning and cooking emissions were assigned to non-fossil WSOC fraction (see Sec.
167 2.5). Meanwhile, the remaining WSOC fractions are assigned to the secondary factors, which
168 can be from both fossil and non-fossil origins, were considered collectively and compared to



169 the unassigned fossil and non-fossil WSOC, to retrieve the origins of this remaining fraction
170 (see Sec. 2.5).

171 **2.4 ¹⁴C measurement of WSOC**

172 ¹⁴C content of micro-scale WSOC aerosol samples was measured with a newly
173 developed method (Zhang et al., 2014c). Briefly, a 16-mm-diameter punch of each filter was
174 extracted using 10 ml ultrapure water with low TOC impurity (less than 5 ppb). The water
175 extracts were recovered in the 20 ml PFA vials and were then pre-frozen at -20 °C more than 5
176 hours before completely dryness in a freeze dryer (Alpha 2-4 LSC, Christ, Germany) for about
177 24 h to 36 h. The residue was re-dissolved in 50 µl of ultrapure water three times and transferred
178 into 200 µl tin capsules (Elementar, Germany). The concentrated samples were heated in the
179 oven at 55-60 °C until complete dryness before the ¹⁴C measurements.

180 WSOC extracts in tin capsules were then converted to CO₂ by the oxidation of the
181 carbon-containing samples using an Elemental Analyzer (EA, Model Vario Micro, Elementar,
182 Germany) as a combustion unit (up to 1050 °C). The resulting CO₂ was introduced continuously
183 by a versatile gas inlet system into a gas ion source of the accelerator mass spectrometer
184 MICADAS where ¹⁴C of CO₂ was finally measured (Wacker et al., 2013; Salazar et al., 2015).
185 The ¹⁴C content of OC and EC was measured in our previous study (Zhang et al., 2015). ¹⁴C
186 results were expressed as fraction of modern (f_M), i.e., the fraction of the measured ¹⁴C/¹²C ratio
187 related to the ¹⁴C/¹²C ratio of the reference year 1950 (Stuiver, 1977). To correct excess ¹⁴C
188 from nuclear bomb tests in the 1950s and 1960s, f_M values were converted to the fraction of
189 non-fossil (f_{NF}) (Zotter et al., 2014a; Zhang et al., 2012):

$$190 \quad f_{NF} = f_M / f_{M,ref} \text{ (Eq. 3)}$$

191 $f_{M,ref}$ is a reference value of f_M for non-fossil carbon sources including biogenic and
192 biomass burning emissions, which were estimated as 1.08 ± 0.05 for WSOC samples collected
193 in 2013 according to the contemporary atmospheric CO₂ f_M (Levin et al., 2010) and a tree
194 growth model (Mohn et al., 2008).



195 2.5 AMS²-based source apportionment of WSOC

196 To better understand the origin of WSOC observed at these sites, WSOC sources were
197 apportioned into several major sources by a combination of ¹⁴C and PMF source
198 apportionments (See Figure 1). Here, two “AMS” (i.e., accelerator mass spectrometer and
199 aerosol mass spectrometer), such a combined approach was named as “AMS²-based source
200 apportionment.

201 WSOC concentration from non-fossil (WSOC_{NF}) and fossil (WSOC_F) sources were
202 calculated from:

$$203 \text{WSOC}_{\text{NF}} = \text{WSOC} * f_{\text{NF}}(\text{WSOC}) \text{ (Eq. 4)}$$

$$204 \text{WSOC}_{\text{F}} = \text{WSOC} - \text{WSOC}_{\text{NF}} \text{ (Eq. 5)}$$

205 The mass concentration of WSOC was derived from the subtraction of TC mass
206 measured from a water-extracted filter from that measured with an un-treated filter (Zhang et
207 al., 2012):

$$208 \text{WSOC} = \text{TC}_{\text{un-treated}} - \text{TC}_{\text{water-extracted}} \text{ (Eq. 6)}$$

209 Based on mass balance, WIOC concentrations from non-fossil (WIOC_{NF}) and fossil
210 (WIOC_F) sources were calculated from:

$$211 \text{WIOC}_{\text{NF}} = \text{OC}_{\text{NF}} - \text{WSOC}_{\text{NF}} \text{ (Eq. 7)}$$

$$212 \text{WIOC}_{\text{F}} = \text{OC}_{\text{F}} - \text{WSOC}_{\text{F}} \text{ (Eq. 8)}$$

213 where OC concentrations from non-fossil (OC_{NF}) and fossil (OC_F) sources were
214 obtained by mass and ¹⁴C measurement of the OC fraction, which were reported previously
215 (Zhang et al., 2015).

216 The non-fossil and fossil-fuel derived WSOC can be apportioned into primary and
217 secondary OC:



218
$$\text{WSOC}_{\text{NF}} = \text{WSOC}_{\text{POC,NF}} + \text{WSOC}_{\text{SOC,NF}} \text{ (Eq.9)}$$

219
$$\text{WSOC}_{\text{F}} = \text{WSOC}_{\text{POC,F}} + \text{WSOC}_{\text{SOC,F}} \text{ (Eq.10)}$$

220 $\text{WSOC}_{\text{POC,NF}}$ can be sub-divided into the following three major primary emissions including
221 cooking emission (WSOC_{CI}) and biomass burning (WSOC_{BB}).

222
$$\text{WSOC}_{\text{POC,NF}} = \text{WSOC}_{\text{CI}} + \text{WSOC}_{\text{BB}} \text{ (Eq.11)}$$

223 Similarly, $\text{WSOC}_{\text{POC,F}}$ can be sub-divided into the following two major primary emissions
224 including traffic (WSOC_{TR}) and coal combustion (WSOC_{CB}).

225
$$\text{WSOC}_{\text{POC,F}} = \text{WSOC}_{\text{TR}} + \text{WSOC}_{\text{CB}} \text{ (Eq.12)}$$

226 where primary fractions such as WSOC_{CI} , WSOC_{BB} , WSOC_{TR} and WSOC_{CB} are
227 previously estimated by the off-line AMS-PMF approach (Huang et al., 2014; Daellenbach et
228 al., 2016; Bozzetti et al., 2017a; Bozzetti et al., 2017b).

229 An uncertainty propagation scheme using a Latin-hypercube sampling (LHS) model
230 was implemented to properly estimate overall uncertainties including measurement
231 uncertainties of the mass determinations of carbon species (i.e., OC, EC, TC, WSOC, WIOC)
232 and ^{14}C measurement, blank corrections from field blanks, and estimation of $f_{\text{M,ref}}$ (Zhang et al.,
233 2015).

234 **3 RESULTS AND DISCUSSION**

235 **3.1 Overall results**

236 During the haze periods of January 2013, the highest daily average $\text{PM}_{2.5}$ concentrations were
237 found in Xi'an ($345 \mu\text{g}/\text{m}^3$) followed by Beijing ($158 \mu\text{g}/\text{m}^3$), Shanghai ($90 \mu\text{g}/\text{m}^3$) and
238 Guangzhou ($68 \mu\text{g}/\text{m}^3$). These levels were much higher than the China's National ambient Air
239 quality standards (i.e., $35 \mu\text{g}/\text{m}^3$). Indeed, several studies have already reported the chemical
240 composition, source and formation mechanism of $\text{PM}_{2.5}$ in many large cities during the haze
241 events of January 2013 in East China. For examples, Huang et al. (2014) revealed that the



242 secondary aerosol formation contributed to 44–71% of OA in Beijing, Xi'an, Shanghai, and
243 Guangzhou during this extremely haze event in China (Huang et al., 2014). By ^{14}C -based source
244 appointment conducted in the same campaign, Zhang et al. (2015) have reported that
245 carbonaceous aerosol pollution was driven to a large (often dominant) extent by SOA formation
246 from both, fossil and biomass-burning sources (Zhang et al., 2015). For all four cities, the 24 h
247 average levels of WSOC were significantly correlated with the levels of $\text{PM}_{2.5}$ and OC ($R=0.99$,
248 $p<0.01$, Figure 2), suggesting that WSOC and OA may have similar sources and formation
249 processes and thus have important implications for OC loadings and associated environmental
250 and health effects. However, the sources of WSOC remain poorly constrained. In this study,
251 we measured the ^{14}C content of WSOC aerosols in six samples (three with the highest three
252 with average PM mass) for each city to report on heavily and moderately polluted days (HPD
253 and MPD, respectively) (Zhang et al., 2015). The ^{14}C contents of OC and EC of the same
254 samples were reported previously (Zhang et al., 2015).

255 WSOC on average accounted for $53\pm 8.0\%$ (ranging from 40–65%) of OC including all samples
256 from the four sites, which was consistent with previous estimates. Based on these
257 measurements, the concentrations of WSOC from non-fossil sources (WSOC_{NF}) spanned from
258 1.41 to $45.3 \mu\text{g}/\text{m}^3$ with a mean of $10.6\pm 12.1 \mu\text{g}/\text{m}^3$, whereas the corresponding range for
259 WSOC from fossil-fuel emissions (WSOC_{F}) was 0.44 to $20.1 \mu\text{g}/\text{m}^3$ with a mean of 5.3 ± 4.9
260 $\mu\text{g}/\text{m}^3$ (Figure 3). Similar to $\text{PM}_{2.5}$ levels, the highest concentrations of WSOC_{NF} and WSOC_{F}
261 were observed in Northern China in Xi'an and Beijing (Xi'an>Beijing), followed by the two
262 southern sites Shanghai and Guangzhou. Non-fossil contributions (mean \pm standard deviation)
263 to total WSOC were $53\pm 5\%$, $75\pm 4\%$, $48\pm 2\%$ and $68\pm 6\%$ in Beijing, Xi'an, Shanghai, and
264 Guangzhou, respectively. Thus, fossil contributions were notably higher in Beijing and
265 Shanghai than those in Xi'an and Guangzhou. Such a trend was also observed for OC (Zhang
266 et al., 2015), suggesting relatively high contribution from fossil-fuel emissions to OC and
267 WSOC due to large coal usage. Despite of these fossil emissions, non-fossil sources were
268 considerably important or even dominant contributors for all the studied sites, which may be



269 associated with primary and secondary OA from regional-transported and local biomass
270 burning emissions. It should also be noted that formation of SOA derived from biogenic VOCs
271 may also have contributed to WSOC_{NF} in Guangzhou, where temperatures during the sampling
272 period were significantly higher (i.e., 5–18 °C) than those in other cities (i.e., -12 to
273 +9 °C)(Bozzetti et al., 2017b). Although both fossil and non-fossil WSOC concentrations were
274 dramatically enhanced during HPD compared to those during MPD, their relative contributions
275 did not change significantly in Beijing and Shanghai whereas a small increasing and decreasing
276 trend in non-fossil fraction was found in Xi'an and Guangzhou, respectively (Figure 3). This
277 suggests that the source pattern of WSOC in Beijing and Shanghai remained similar between
278 HPD and MPD, but the increase in the WSOC concentrations was rather enhanced by additional
279 fossil-fuel and biogenic/biomass burning emissions in Guangzhou and Xi'an, respectively. It
280 should be noted that the meteorological conditions play significant roles on the haze formation
281 in the eastern China during winter 2013, and has already been well documented (Zhang et al.,
282 2014a). However, the details sources of WSOC and WIOC were still unclear.

283 3.2 WSOC versus WIOC

284 To compare sources of WSOC and WIOC aerosols, the mass concentrations and ¹⁴C contents
285 of WIOC were also derived based on mass balance. The ¹⁴C-based source apportionment of
286 WIOC and the relationship between $f_{NF}(WSOC)$ and $f_{NF}(WIOC)$ is presented in Figures 4 and
287 5a, respectively. It shows that non-fossil contributions to WSOC were larger than those of
288 WIOC for nearly all samples in Beijing, Xi'an and Guangzhou. On average, the majority (60-
289 70%) of the fossil OC was water insoluble at these 3 sites (see Figure 5b), indicating that fossil-
290 derived OA mostly consisted of hydrophobic components and thus is less water soluble than
291 OA from non-fossil sources. This result is consistent with findings reported elsewhere such as
292 at an urban or rural site in Switzerland (Zhang et al., 2013), a remote site in Hainan Island,
293 South China (Zhang et al., 2014b) and at two rural sites on the east coast of the United States
294 (Wozniak et al., 2012). Meanwhile, the fossil OC in Shanghai, the dominant fraction of OC,
295 was more water soluble (Figure 5b), suggesting an enhanced SOA formation from fossil VOCs



296 from vehicle emissions and/or coal burning for this city. As shown in Figure 5b, non-fossil OA
297 was enriched in water-soluble fractions (i.e., $60\% \pm 8\%$) for all cities, associated with the
298 hydrophilic properties of biogenic-derived SOA and biomass-burning derived primary organic
299 aerosol (POA) and SOA, which are composed of a large fraction of polar and highly oxygenated
300 compounds (Mayol-Bracero et al., 2002; Sullivan et al., 2011; Noziere et al., 2015). Thus, non-
301 fossil OC has more water-soluble components than fossil ones. It should be noted that relative
302 contributions of $WSOC_{NF}$ and $WSOC_F$ are similar in Beijing and Shanghai, whereas $WSOC_{NF}$
303 is much higher than $WSOC_F$ in Xi'an and Guangzhou. This suggests larger contribution of non-
304 fossil sources to WSOC aerosols in Xi'an and Guangzhou than those in Beijing and Shanghai.

305 **3.3 High contribution of secondary formation to WSOC**

306 WSOC was further apportioned into fossil sources such as coal burning (CB), traffic (TR) and
307 SOC (SOC,F) as well as non-fossil sources such as biomass burning (BB), cooking (CI) and
308 SOC (SOC,NF) using a AMS² based source apportionment (see Sec. 2.5 and Figure 1). SOC
309 dominated WSOC during both the HPD and MPD with a mean contribution of $67\% \pm 9\%$,
310 highlighting the importance of SOC formation to the WSOC aerosols in wintertime pollution
311 events. This is consistent with our previous findings for total PM_{2.5} mass and bulk carbonaceous
312 aerosols (i.e., total carbon, sum of OC and EC) (Huang et al., 2014; Zhang et al., 2015). The
313 increase in SOC contribution to WSOC during HPD compared to MPD can be largely due to
314 fossil contribution in Beijing but non-fossil emissions in Xi'an. In Shanghai and Guangzhou,
315 the source pattern of WSOC was not significantly different between MPD and HPD. Fossil
316 contributions to $WSOC_{SOC}$ were $50\% \pm 9\%$ in Beijing, $61\% \pm 4\%$ in Shanghai, associated with SOA
317 from local and transported fossil-fuel derived precursors at these sites (Guo et al., 2014). This
318 contribution drops to $36\% \pm 9\%$ and $26\% \pm 9\%$ in Guangzhou and Xi'an, respectively, due to higher
319 biomass-burning contribution to SOC. Despite of the general importance of fossil SOC,
320 formation of non-fossil $WSOC_{SOC}$ becomes especially relevant during HPD especially in Xi'an
321 (Figure 6), which may be explained by competing effects in SOC formation from fossil versus
322 non-fossil precursors. It can be hypothesized for extremely polluted episodes that more



323 hydrophilic volatile compounds that were emitted from biomass burning precursors
324 preferentially form SOC compounds via heterogeneous reaction/processing on dust particles
325 compared to highly hydrophobic precursors from fossil sources, a point subjected to future
326 laboratory and field experiments. The most important primary sources of WSOC were biomass
327 burning emissions, and their contributions were higher in Xi'an ($26\% \pm 7\%$) and Guangzhou
328 ($25\% \pm 6\%$) than those found in Beijing ($17\% \pm 6\%$) and Shanghai ($17\% \pm 5\%$). The remaining
329 primary sources such as coal combustion, cooking and traffic were generally very small
330 contributors of WSOC due to lower water solubility, although coal combustion could exceed
331 10% in Beijing. It should be noted that WSOC was dominated by SOC formation with mean
332 contribution of $61\% \pm 10\%$ and $72\% \pm 12\%$ (average for all four cities) to non-fossil and fossil-
333 fuel derived WSOC, respectively.

334 **Summary and implications**

335 Our study demonstrates that non-fossil emissions are generally a dominant contributor of
336 WSOC aerosols during extreme haze events in representative major cities of China, which is in
337 agreement with WSOC source information identified in aerosols with different size fractions
338 (e.g., TSP, PM_{10} and $PM_{2.5}$) observed in the Northern Hemisphere at urban, rural, semi-urban,
339 and background sites in East/South Asia, Europe and USA (Table 1). The ^{14}C -based source
340 apportionment database shows a mean non-fossil fraction of $73 \pm 11\%$ across all sites. This
341 overwhelming non-fossil contribution to WSOC is consistently observed throughout the year,
342 which is associated with seasonal-dependent biomass-burning emissions and/or biogenic-
343 derived SOC formation. Our study provides evidence that the presence of oxidized OA, which
344 is to a large extent water soluble, in the Northern Hemisphere (Zhang et al., 2007) is mainly
345 derived from biogenic-derived SOA and/or biomass burning sources. The overall importance
346 of non-fossil emissions to the WSOC aerosols results from large contributions of SOC
347 formation from biogenic precursors (e.g., most likely during summer) and relatively high water-
348 solubility of primary biomass burning particles (e.g., most likely during winter) compared to
349 those emitted from fossil fuel emissions such as coal combustion and vehicle exhaust. Despite



350 of the importance of non-fossil sources, a significant fossil fraction is also observed in the
351 WSOC aerosols from polluted regions in East Asia and sites influenced by East Asian
352 continental outflow (Table 1, Figure 7). This fossil contribution is apparently higher than in this
353 region than in the USA and Europe, which is due to large industrial and residential coal usage
354 as well as vehicle emissions. From our observation, the increases in the fossil fractions of
355 WSOC were mostly from SOC formation. Since WSOC has hygroscopic properties, our
356 findings suggest that SOC formation from non-fossil emissions have significant implications
357 on aerosol-induced climate effects. In addition, fossil-derived SOC formation may also become
358 important in polluted regions with large amounts of fossil fuel emissions such as in China and
359 other emerging countries. Low combustion efficiencies and consequently high emission factors
360 in most of the combustion processes in China may further be responsible for increased
361 concentrations of fossil precursors which may be oxidized to form water-soluble SOA in the
362 atmosphere and contribute substantially to the WSOC aerosols. The enhanced WSOC levels
363 may be also originate from aging of fossil POA during the long-range transport of aerosols
364 (Kirillova et al., 2014a). It is also interesting to note that fossil contribution during winter in
365 East Asia is generally higher than those in the rest of the year although relatively large fossil
366 fraction could be occasionally found as well. Such seasonal dependence was not observed in
367 other regions, suggesting the importance of fossil contribution to WSOC due to increasing coal
368 combustions during winter in China. This study provides a more detailed source apportionment
369 of WSOC, which could improve modelling of climate and health effects as well as the
370 understanding of atmospheric chemistry of WSOC in the polluted atmosphere such as China
371 and provide scientific basis for policy decisions on air pollution emissions mitigation.

372 REFERENCES

- 373 Andreae, M. O., and Gelencser, A.: Black carbon or brown carbon? The nature of light-
374 absorbing carbonaceous aerosols, *Atmos. Chem. Phys.*, 6, 3131-3148, 2006.
- 375 Asa-Awuku, A., Moore, R. H., Nenes, A., Bahreini, R., Holloway, J. S., Brock, C. A.,
376 Middlebrook, A. M., Ryerson, T. B., Jimenez, J. L., DeCarlo, P. F., Hecobian, A., Weber, R.



- 377 J., Stickel, R., Tanner, D. J., and Huey, L. G.: Airborne cloud condensation nuclei
378 measurements during the 2006 Texas Air Quality Study, *J. Geophys. Res.*, 116, D11201, 2011.
- 379 Bosch, C., Andersson, A., Kirillova, E. N., Budhavant, K., Tiwari, S., Praveen, P. S., Russell,
380 L. M., Beres, N. D., Ramanathan, V., and Gustafsson, O.: Source-diagnostic dual-isotope
381 composition and optical properties of water-soluble organic carbon and elemental carbon in the
382 South Asian outflow intercepted over the Indian Ocean, *J. Geophys. Res.*, 119, 11743-11759,
383 2014.
- 384 Bozzetti, C., El Haddad, I., Salameh, D., Daellenbach, K. R., Fermo, P., Gonzalez, R.,
385 Minguillón, M. C., Iinuma, Y., Poulain, L., Elser, M., Müller, E., Slowik, J. G., Jaffrezo, J. L.,
386 Baltensperger, U., Marchand, N., and Prévôt, A. S. H.: Organic aerosol source apportionment
387 by offline-AMS over a full year in Marseille, *Atmos. Chem. Phys.*, 17, 8247-8268, 2017a.
- 388 Bozzetti, C., Sosedova, Y., Xiao, M., Daellenbach, K. R., Ulevicius, V., Dudoitis, V., Mordas,
389 G., Byčenkienė, S., Plauškaitė, K., Vlachou, A., Golly, B., Chazeau, B., Besombes, J. L.,
390 Baltensperger, U., Jaffrezo, J. L., Slowik, J. G., El Haddad, I., and Prévôt, A. S. H.: Argon
391 offline-AMS source apportionment of organic aerosol over yearly cycles for an urban, rural,
392 and marine site in northern Europe, *Atmos. Chem. Phys.*, 17, 117-141, 2017b.
- 393 Canonaco, F., Crippa, M., Slowik, J. G., Baltensperger, U., and Prévôt, A. S. H.: SoFi, an
394 IGOR-based interface for the efficient use of the generalized multilinear engine (ME-2) for the
395 source apportionment: ME-2 application to aerosol mass spectrometer data, *Atmos. Meas.*
396 *Tech.*, 6, 3649-3661, 2013.
- 397 Cao, F., Zhang, Y.-L., Szidat, S., Zapf, A., Wacker, L., and Schwikowski, M.: Microgram-level
398 radiocarbon determination of carbonaceous particles in firn and ice samples: pretreatment and
399 OC/EC separation, *Radiocarbon*, 55, 383-390, 2013.
- 400 Cavalli, F., Viana, M., Yttri, K. E., Genberg, J., and Putaud, J. P.: Toward a standardised
401 thermal-optical protocol for measuring atmospheric organic and elemental carbon: the
402 EUSAAR protocol, *Atmos. Meas. Tech.*, 3, 79-89, 2010.
- 403 Cheng, Y., He, K. B., Zheng, M., Duan, F. K., Du, Z. Y., Ma, Y. L., Tan, J. H., Yang, F. M.,
404 Liu, J. M., Zhang, X. L., Weber, R. J., Bergin, M. H., and Russell, A. G.: Mass absorption



405 efficiency of elemental carbon and water-soluble organic carbon in Beijing, China, Atmos.
406 Chem. Phys., 11, 11497-11510, 2011.

407 Daellenbach, K. R., Bozzetti, C., Krepelova, A. K., Canonaco, F., Wolf, R., Zotter, P., Fermo,
408 P., Crippa, M., Slowik, J. G., Sosedova, Y., Zhang, Y., Huang, R. J., Poulain, L., Szidat, S.,
409 Baltensperger, U., El Haddad, I., and Prevot, A. S. H.: Characterization and source
410 apportionment of organic aerosol using offline aerosol mass spectrometry, Atmos. Meas. Tech.,
411 9, 23-39, 2016.

412 Fang, W., Andersson, A., Zheng, M., Lee, M., Holmstrand, H., Kim, S.-W., Du, K., and
413 Gustafsson, Ö.: Divergent Evolution of Carbonaceous Aerosols during Dispersal of East Asian
414 Haze, Scientific Reports, 7, 10422, 2017.

415 Fu, P., Kawamura, K., Chen, J., Qin, M., Ren, L., Sun, Y., Wang, Z., Barrie, L. A., Tachibana,
416 E., Ding, A., and Yamashita, Y.: Fluorescent water-soluble organic aerosols in the High Arctic
417 atmosphere, Sci Rep, 5, 9845, 2015.

418 Guo, S., Hu, M., Zamora, M. L., Peng, J., Shang, D., Zheng, J., Du, Z., Wu, Z., Shao, M., Zeng,
419 L., Molina, M. J., and Zhang, R.: Elucidating severe urban haze formation in China, Proc. Nat.
420 Acad. Sci. U.S.A., 111, 17373-17378, 2014.

421 Hecobian, A., Zhang, X., Zheng, M., Frank, N., Edgerton, E. S., and Weber, R. J.: Water-
422 Soluble Organic Aerosol material and the light-absorption characteristics of aqueous extracts
423 measured over the Southeastern United States, Atmos. Chem. Phys., 10, 5965-5977, 2010.

424 Huang, R. J., Zhang, Y., Bozzetti, C., Ho, K. F., Cao, J. J., Han, Y., Daellenbach, K. R., Slowik,
425 J. G., Platt, S. M., Canonaco, F., Zotter, P., Wolf, R., Pieber, S. M., Bruns, E. A., Crippa, M.,
426 Ciarelli, G., Piazzalunga, A., Schwikowski, M., Abbaszade, G., Schnelle-Kreis, J.,
427 Zimmermann, R., An, Z., Szidat, S., Baltensperger, U., El Haddad, I., and Prevot, A. S.: High
428 secondary aerosol contribution to particulate pollution during haze events in China, Nature, 514,
429 218-222, 2014.

430 Jimenez, J. L., Canagaratna, M. R., Donahue, N. M., Prevot, A. S. H., Zhang, Q., Kroll, J. H.,
431 DeCarlo, P. F., Allan, J. D., Coe, H., Ng, N. L., Aiken, A. C., Docherty, K. S., Ulbrich, I. M.,
432 Grieshop, A. P., Robinson, A. L., Duplissy, J., Smith, J. D., Wilson, K. R., Lanz, V. A., Hueglin,



433 C., Sun, Y. L., Tian, J., Laaksonen, A., Raatikainen, T., Rautiainen, J., Vaattovaara, P., Ehn,
434 M., Kulmala, M., Tomlinson, J. M., Collins, D. R., Cubison, M. J., Dunlea, E. J., Huffman, J.
435 A., Onasch, T. B., Alfarra, M. R., Williams, P. I., Bower, K., Kondo, Y., Schneider, J.,
436 Drewnick, F., Borrmann, S., Weimer, S., Demerjian, K., Salcedo, D., Cottrell, L., Griffin, R.,
437 Takami, A., Miyoshi, T., Hatakeyama, S., Shimono, A., Sun, J. Y., Zhang, Y. M., Dzepina, K.,
438 Kimmel, J. R., Sueper, D., Jayne, J. T., Herndon, S. C., Trimborn, A. M., Williams, L. R., Wood,
439 E. C., Middlebrook, A. M., Kolb, C. E., Baltensperger, U., and Worsnop, D. R.: Evolution of
440 organic aerosols in the atmosphere, *Science*, 326, 1525-1529, 2009.

441 Kirillova, E. N., Sheesley, R. J., Andersson, A., and Gustafsson, O.: Natural abundance ^{13}C and
442 ^{14}C analysis of water-soluble organic carbon in atmospheric aerosols, *Anal. Chem.*, 82, 7973-
443 7978, 2010.

444 Kirillova, E. N., Andersson, A., Sheesley, R. J., Kruså, M., Praveen, P. S., Budhavant, K., Safai,
445 P. D., Rao, P. S. P., and Gustafsson, Ö.: ^{13}C and ^{14}C -based study of sources and atmospheric
446 processing of water-soluble organic carbon (WSOC) in South Asian aerosols, *J. Geophys. Res.*,
447 118, 614-626, 2013.

448 Kirillova, E. N., Andersson, A., Han, J., Lee, M., and Gustafsson, O.: Sources and light
449 absorption of water-soluble organic carbon aerosols in the outflow from northern China, *Atmos.*
450 *Chem. Phys.*, 14, 1413-1422, 2014a.

451 Kirillova, E. N., Andersson, A., Tiwari, S., Srivastava, A. K., Bisht, D. S., and Gustafsson, O.:
452 Water-soluble organic carbon aerosols during a full New Delhi winter: Isotope-based source
453 apportionment and optical properties, *J. Geophys. Res.*, 119, 3476-3485, 2014b.

454 Kondo, Y., Miyazaki, Y., Takegawa, N., Miyakawa, T., Weber, R. J., Jimenez, J. L., Zhang,
455 Q., and Worsnop, D. R.: Oxygenated and water-soluble organic aerosols in Tokyo, *J. Geophys.*
456 *Res.*, 112, D01203, 2007.

457 Laskin, A., Laskin, J., and Nizkorodov, S. A.: Chemistry of Atmospheric Brown Carbon, *Chem.*
458 *Rev. (Washington, DC, U. S.)*, 115, 4335-4382, 2015.



- 459 Levin, I., Naegler, T., Kromer, B., Diehl, M., Francey, R. J., Gomez-Pelaez, A. J., Steele, L. P.,
460 Wagenbach, D., Weller, R., and Worthy, D. E.: Observations and modelling of the global
461 distribution and long-term trend of atmospheric $^{14}\text{CO}_2$, *Tellus B*, 62, 26-46, 2010.
- 462 Limbeck, A., Handler, M., Neuberger, B., Klatzer, B., and Puxbaum, H.: Carbon-specific
463 analysis of humic-like substances in atmospheric aerosol and precipitation samples, *Anal.*
464 *Chem.*, 77, 7288-7293, 2005.
- 465 Liu, J., Li, J., Vonwiller, M., Liu, D., Cheng, H., Shen, K., Salazar, G., Agrios, K., Zhang, Y.,
466 He, Q., Ding, X., Zhong, G., Wang, X., Szidat, S., and Zhang, G.: The importance of non-fossil
467 sources in carbonaceous aerosols in a megacity of central China during the 2013 winter haze
468 episode: A source apportionment constrained by radiocarbon and organic tracers, *Atmos.*
469 *Environ.*, 144, 60-68, 2016.
- 470 Liu, J. W., Li, J., Zhang, Y. L., Liu, D., Ding, P., Shen, C. D., Shen, K. J., He, Q. F., Ding, X.,
471 Wang, X. M., Chen, D. H., Szidat, S., and Zhang, G.: Source Apportionment Using
472 Radiocarbon and Organic Tracers for PM_{2.5} Carbonaceous Aerosols in Guangzhou, South
473 China: Contrasting Local- and Regional-Scale Haze Events, *Environ. Sci. Technol.*, 48, 12002-
474 12011, 2014.
- 475 Mayol-Bracero, O. L., Guyon, P., Graham, B., Roberts, G., Andreae, M. O., Decesari, S.,
476 Facchini, M. C., Fuzzi, S., and Artaxo, P.: Water-soluble organic compounds in biomass
477 burning aerosols over Amazonia - 2. Apportionment of the chemical composition and
478 importance of the polyacidic fraction, *J. Geophys. Res.*, 107, D8091, 2002.
- 479 Miyazaki, Y., Kondo, Y., Takegawa, N., Komazaki, Y., Fukuda, M., Kawamura, K., Mochida,
480 M., Okuzawa, K., and Weber, R. J.: Time-resolved measurements of water-soluble organic
481 carbon in Tokyo, *J. Geophys. Res.*, 111, D23206, 2006.
- 482 Mohn, J., Szidat, S., Fellner, J., Rechberger, H., Quartier, R., Buchmann, B., and Emmenegger,
483 L.: Determination of biogenic and fossil CO_2 emitted by waste incineration based on $^{14}\text{CO}_2$ and
484 mass balances, *Bioresour. Technol.*, 99, 6471-6479, 2008.
- 485 Noziere, B., Kalberer, M., Claeys, M., Allan, J., D'Anna, B., Decesari, S., Finessi, E., Glasius,
486 M., Grgic, I., Hamilton, J. F., Hoffmann, T., Iinuma, Y., Jaoui, M., Kahnt, A., Kampf, C. J.,



487 Kourtchev, I., Maenhaut, W., Marsden, N., Saarikoski, S., Schnelle-Kreis, J., Surratt, J. D.,
488 Szidat, S., Szmigielski, R., and Wisthaler, A.: The molecular identification of organic
489 compounds in the atmosphere: state of the art and challenges, *Chem Rev*, 115, 3919-3983, 2015.
490 Pavuluri, C. M., Kawamura, K., Uchida, M., Kondo, M., and Fu, P. Q.: Enhanced modern
491 carbon and biogenic organic tracers in Northeast Asian aerosols during spring/summer, *J.*
492 *Geophys. Res.*, 118, 2362-2371, 2013.
493 Ruellan, S., and Cachier, H.: Characterisation of fresh particulate vehicular exhausts near a
494 Paris high flow road, *Atmos. Environ.*, 35, 453-468, 2001.
495 Salazar, G., Zhang, Y. L., Agrios, K., and Szidat, S.: Development of a method for fast and
496 automatic radiocarbon measurement of aerosol samples by online coupling of an elemental
497 analyzer with a MICADAS AMS, *Nucl. Instr. and Meth. in Phys. Res. B.*, 361, 163-167, 2015.
498 Sannigrahi, P., Sullivan, A. P., Weber, R. J., and Ingall, E. D.: Characterization of water-soluble
499 organic carbon in urban atmospheric aerosols using solid-state C-13 NMR spectroscopy,
500 *Environ. Sci. Technol.*, 40, 666-672, 2006.
501 Stuiver, M.: Discussion: Reporting of ^{14}C data, *Radiocarbon*, 19, 355-363, 1977.
502 Sullivan, A. P., Frank, N., Kenski, D. M., and Collett, J. L.: Application of high-performance
503 anion-exchange chromatography-pulsed amperometric detection for measuring carbohydrates
504 in routine daily filter samples collected by a national network: 2. Examination of sugar
505 alcohols/polyols, sugars, and anhydrosugars in the upper Midwest, *J. Geophys. Res.*, 116,
506 D08303, 2011.
507 Szidat, S., Jenk, T. M., Gäggeler, H. W., Synal, H. A., Fisseha, R., Baltensperger, U., Kalberer,
508 M., Samburova, V., Wacker, L., Saurer, M., Schwikowski, M., and Hajdas, I.: Source
509 apportionment of aerosols by ^{14}C measurements in different carbonaceous particle fractions,
510 *Radiocarbon*, 46, 475-484, 2004.
511 Szidat, S., Ruff, M., Perron, N., Wacker, L., Synal, H.-A., Hallquist, M., Shannigrahi, A. S.,
512 Yttri, K. E., Dye, C., and Simpson, D.: Fossil and non-fossil sources of organic carbon (OC)
513 and elemental carbon (EC) in Goeteborg, Sweden, *Atmos. Chem. Phys.*, 9, 1521-1535, 2009.



- 514 Timonen, H., Carbone, S., Aurela, M., Saarnio, K., Saarikoski, S., Ng, N. L., Canagaratna, M.
515 R., Kulmala, M., Kerminen, V. M., Worsnop, D. R., and Hillamo, R.: Characteristics, sources
516 and water-solubility of ambient submicron organic aerosol in springtime in Helsinki, Finland,
517 *J. Aerosol Sci.*, 56, 61-77, 2013.
- 518 Wacker, L., Fahrni, S. M., Hajdas, I., Molnar, M., Synal, H. A., Szidat, S., and Zhang, Y. L.: A
519 versatile gas interface for routine radiocarbon analysis with a gas ion source, *Nucl. Instrum.*
520 *Meth. B*, 294, 315-319, 2013.
- 521 Weber, R. J., Sullivan, A. P., Peltier, R. E., Russell, A., Yan, B., Zheng, M., de Gouw, J.,
522 Warneke, C., Brock, C., Holloway, J. S., Atlas, E. L., and Edgerton, E.: A study of secondary
523 organic aerosol formation in the anthropogenic-influenced southeastern United States, *J.*
524 *Geophys. Res.*, 112, D13302, 2007.
- 525 Wozniak, A. S., Bauer, J. E., and Dickhut, R. M.: Characteristics of water-soluble organic
526 carbon associated with aerosol particles in the eastern United States, *Atmos. Environ.*, 46, 181-
527 188, 2012.
- 528 Xiao, R., Takegawa, N., Zheng, M., Kondo, Y., Miyazaki, Y., Miyakawa, T., Hu, M., Shao, M.,
529 Zeng, L., Gong, Y., Lu, K., Deng, Z., Zhao, Y., and Zhang, Y. H.: Characterization and source
530 apportionment of submicron aerosol with aerosol mass spectrometer during the PRIDE-PRD
531 2006 campaign, *Atmos. Chem. Phys.*, 11, 6911-6929, 2011.
- 532 Yan, C., Zheng, M., Bosch, C., Andersson, A., Desyaterik, Y., Sullivan, A. P., Collett, J. L.,
533 Zhao, B., Wang, S., He, K., and Gustafsson, O.: Important fossil source contribution to brown
534 carbon in Beijing during winter, *Sci Rep*, 7, 43182, 2017.
- 535 Zappoli, S., Andracchio, A., Fuzzi, S., Facchini, M. C., Gelencser, A., Kiss, G., Krivacsy, Z.,
536 Molnar, A., Meszaros, E., Hansson, H. C., Rosman, K., and Zebuhr, Y.: Inorganic, organic and
537 macromolecular components of fine aerosol in different areas of Europe in relation to their
538 water solubility, *Atmos. Environ.*, 33, 2733-2743, 1999.
- 539 Zhang, Q., Jimenez, J. L., Canagaratna, M. R., Allan, J. D., Coe, H., Ulbrich, I., Alfarra, M. R.,
540 Takami, A., Middlebrook, A. M., Sun, Y. L., Dzepina, K., Dunlea, E., Docherty, K., DeCarlo,
541 P. F., Salcedo, D., Onasch, T., Jayne, J. T., Miyoshi, T., Shimono, A., Hatakeyama, S.,



542 Takegawa, N., Kondo, Y., Schneider, J., Drewnick, F., Borrmann, S., Weimer, S., Demerjian,
543 K., Williams, P., Bower, K., Bahreini, R., Cottrell, L., Griffin, R. J., Rautiainen, J., Sun, J. Y.,
544 Zhang, Y. M., and Worsnop, D. R.: Ubiquity and dominance of oxygenated species in organic
545 aerosols in anthropogenically-influenced Northern Hemisphere midlatitudes, *Geophys. Res.*
546 *Letts.*, 34, L13801, 2007.

547 Zhang, R., Li, Q., and Zhang, R.: Meteorological conditions for the persistent severe fog and
548 haze event over eastern China in January 2013, *SCIENCE CHINA Earth Sciences*, 57, 26-35,
549 2014a.

550 Zhang, Y.-L., Li, J., Zhang, G., Zotter, P., Huang, R.-J., Tang, J.-H., Wacker, L., Prévôt, A. S.
551 H., and Szidat, S.: Radiocarbon-based source apportionment of carbonaceous aerosols at a
552 regional background site on hainan Island, South China, *Environ. Sci. Technol.*, 48, 2651-2659,
553 2014b.

554 Zhang, Y.-L., Liu, J.-W., Salazar, G. A., Li, J., Zotter, P., Zhang, G., Shen, R.-r., Schäfer, K.,
555 Schnelle-Kreis, J., Prévôt, A. S. H., and Szidat, S.: Micro-scale (μg) radiocarbon analysis of
556 water-soluble organic carbon in aerosol samples, *Atmos. Environ.*, 97, 1-5, 2014c.

557 Zhang, Y. L., Perron, N., Ciobanu, V. G., Zotter, P., Minguillón, M. C., Wacker, L., Prévôt, A.
558 S. H., Baltensperger, U., and Szidat, S.: On the isolation of OC and EC and the optimal strategy
559 of radiocarbon-based source apportionment of carbonaceous aerosols, *Atmos. Chem. Phys.*, 12,
560 10841-10856, 2012.

561 Zhang, Y. L., Zotter, P., Perron, N., Prévôt, A. S. H., Wacker, L., and Szidat, S.: Fossil and
562 non-fossil sources of different carbonaceous fractions in fine and coarse particles by
563 radiocarbon measurement, *Radiocarbon*, 55, 1510-1520, 2013.

564 Zhang, Y. L., Huang, R. J., El Haddad, I., Ho, K. F., Cao, J. J., Han, Y., Zotter, P., Bozzetti, C.,
565 Daellenbach, K. R., Canonaco, F., Slowik, J. G., Salazar, G., Schwikowski, M., Schnelle-Kreis,
566 J., Abbaszade, G., Zimmermann, R., Baltensperger, U., Prévôt, A. S. H., and Szidat, S.: Fossil
567 vs. non-fossil sources of fine carbonaceous aerosols in four Chinese cities during the extreme
568 winter haze episode of 2013, *Atmos. Chem. Phys.*, 15, 1299-1312, 2015.



569 Zotter, P., Ciobanu, V. G., Zhang, Y. L., El-Haddad, I., Macchia, M., Daellenbach, K. R.,
570 Salazar, G. A., Huang, R. J., Wacker, L., Hueglin, C., Piazzalunga, A., Fermo, P., Schwikowski,
571 M., Baltensperger, U., Szidat, S., and Prévôt, A. S. H.: Radiocarbon analysis of elemental and
572 organic carbon in Switzerland during winter-smog episodes from 2008 to 2012 – Part 1: Source
573 apportionment and spatial variability, *Atmos. Chem. Phys.*, 14, 13551-13570, 2014a.

574 Zotter, P., El-Haddad, I., Zhang, Y., Hayes, P. L., Zhang, X., Lin, Y.-H., Wacker, L., Schnelle-
575 Kreis, J., Abbaszade, G., Zimmermann, R., Surratt, J. D., Weber, R., Jimenez, J. L., Szidat, S.,
576 Baltensperger, U., and Prévôt, A. S. H.: Diurnal cycle of fossil and nonfossil carbon using
577 radiocarbon analyses during CalNex, *J. Geophys. Res.*, 119, 6818-6835, 2014b.

578 **Author Contributions:** Y.-L.Z., S.S., R.J.H., J.J.C. and A.S.H.P. designed the study. Y.L.Z.
579 and G.S. perform ^{14}C measurement. Y.L.Z. and S. S. interpreted the ^{14}C data. R.J.H., I.E.H.,
580 C.B. and K.D. performed the offline AMS analysis and interpret the data. Y.-L.Z. and I.E.H.
581 perform ^{14}C -AMS-PMF source apportionments. Y.-L.Z. wrote the paper. All authors reviewed
582 and commented on the paper.

583 **Competing interests:** The authors declare no competing financial interests.

584 **Acknowledgments:** This work was supported by the National Natural Science Foundation of
585 China (Grant Nos. 91644103, 41603104). All data needed to evaluate the conclusions in the
586 paper are present in the paper. Additional data related to this paper may be requested from the
587 authors.



588 **Figures and Tables**

589 **Table 1.** Compilation of literature values of relative fossil-fuel contributions (fossil %) to the
 590 WSOC aerosols in East/South Asia, USA and Europe.

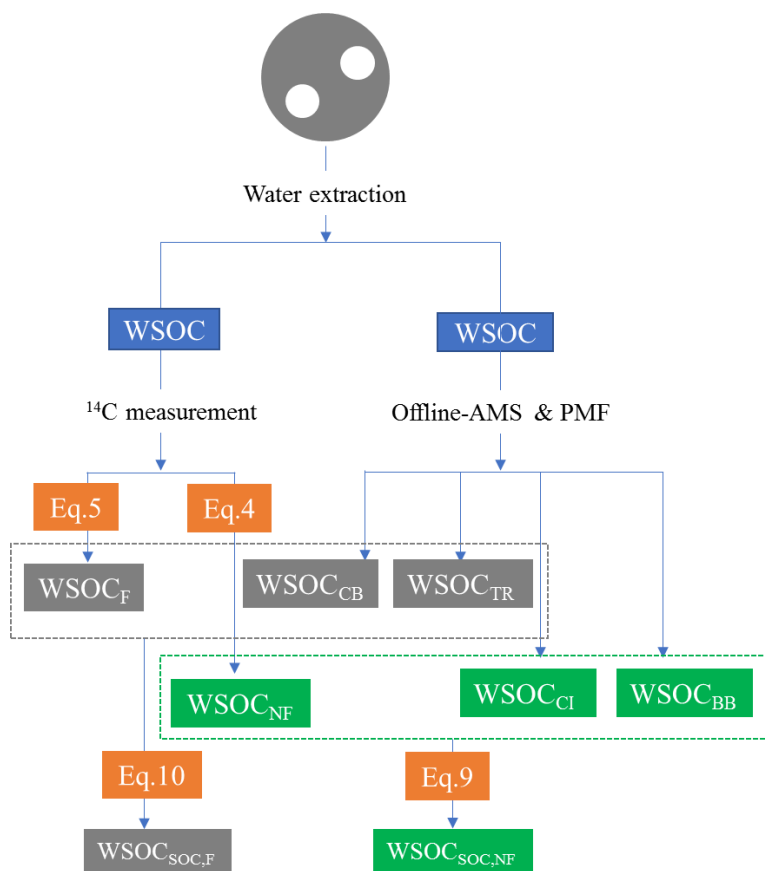
Site	Location	Season	Size	WSOC ($\mu\text{g}/\text{m}^3$)	WSOC/OC	Fossil %	References
East Asia							
Urban	Beijing, China	Winter/2013	PM _{2.5}	19.8	0.49	47	this work
Urban	Xi'an, China	Winter/2013	PM _{2.5}	31.3	0.53	25	this work
Urban	Shanghai, China	Winter/2013	PM _{2.5}	6.5	0.58	52	this work
Urban	Guangzhou, China	Winter/2013	PM _{2.5}	6.6	0.53	32	this work
Urban	Beijing, China	Winter/2014	PM _{2.5}	14.7	0.40	56	(Fang et al., 2017)
Urban	Beijing, China	Winter/2011	PM _{4.3}	15	0.50	55	(Zhang et al., 2014c)
Urban	Beijing, China	Winter/2013	PM _{2.5}	9.3	0.31	54	(Yan et al., 2017)
Urban	Guangzhou, China	Winter/2012/ 2013	PM _{2.5}	4.1	0.38	33	(Liu et al., 2014)
Urban	Guangzhou, China	Winter/2011	PM ₁₀	4.5	0.43	28.5	(Zhang et al., 2014c)
Urban	Xi'an, China	Autumn/2009	PM _{2.5}	5.1	0.28	31	(Pavuluri et al., 2013)
Urban	Xi'an, China	Autumn/2010	TSP	8.1	0.28	29	(Pavuluri et al., 2013)
Urban	Wuhan, China	Winter/2013	PM _{2.5}	13.7	0.45	37	(Liu et al., 2016)
Urban	Sapporo, Japan	Summer/Autumn 2010	PM ₃	1	0.43	15	(Pavuluri et al., 2013)
Urban	Sapporo, Japan	Summer/2011	TSP	1.1	0.24	12	(Pavuluri et al., 2013)
Urban	Sapporo, Japan	Spring/2010	TSP	1.1	0.31	11	(Pavuluri et al., 2013)
Urban	Sapporo, Japan	Autumn/2011	TSP	1.8	0.48	18.3	(Pavuluri et al., 2013)
Urban	Sapporo, Japan	Winter/2010	TSP	0.9	0.45	40.2	(Pavuluri et al., 2013)
Background	Jeju Island, Korea	Winter/2014	PM _{2.5}	2.2	0.66	50	(Fang et al., 2017)
Background	Jeju Island, Korea	Spring/2011	PM _{2.5}	2.0		37.5	(Kirillova et al., 2014a)
Background	Jeju Island, Korea	Spring/2011	TSP	3.0		25	(Kirillova et al., 2014a)
Average						33±14	
South Asia							
Background	Hainan, China	Annual 2005/2006	PM _{2.5}	3.9	0.54	18	(Zhang et al., 2014b)
Background	Hainan, China	Winter 2005/2006	PM _{2.5}	6.2	0.57	14.5	(Zhang et al., 2014b)
Background	Hainan, China	Summer 2005/2006	PM _{2.5}	1.4	0.40	17.7	(Zhang et al., 2014b)
Background	Hanimaadhoo, Maldives	Annual 2008/2009	TSP	0.5		17	(Kirillova et al., 2013)
Background	Sinhagad, India	Annual 2008/2009	TSP	3.0		24	(Kirillova et al., 2013)
Background	Hanimaadhoo, Maldives	Spring/2012	PM _{2.5}	0.6	0.62	14	(Bosch et al., 2014)
Urban	Delhi, India	Winter/2010/ 2011	PM _{2.5}	22.0		21	(Kirillova et al., 2014b)
Average						18±4	



Europe and USA							
Urban	Göteborg, Sweden	Winter/2005	PM _{2.5}	1.1	0.48	23	(Szidat et al., 2009)
Urban	Göteborg, Sweden	Summer/2006	PM _{2.5}	0.8	0.61	30	(Szidat et al., 2009)
Rural	Göteborg, Sweden	Winter/2005		1.2	0.53	27	(Szidat et al., 2009)
Rural/semi-urban	Stockholm, Sweden	Summer/2009	TSP			12	(Kirillova et al., 2010)
Urban	Zürich, Switzerland	Summer/2002	PM ₁₀	2.1	0.54	14	(Szidat et al., 2004)
Urban	Zürich, Switzerland	Winter/2008	PM ₁₀	2.8	0.60	26.8	(Zhang et al., 2013)
Urban	Moleno, Switzerland	Summer/2006	PM ₁₀	5.3	0.67	30	(Zhang et al., 2013)
Urban	Bern, Switzerland	Winter/2009	PM ₁₀		0.39	14	(Zhang et al., 2014c)
Urban	Atlanta, USA	Summer/2004	PM _{2.5}	2.3	0.59	26.5	(Weber et al., 2007)
Rural	Millbrook, USA	Annual/2006/2007	TSP		0.36	12	(Wozniak et al., 2012)
Rural	Harcum, USA	Annual/2006/2007	TSP		0.38	14	(Wozniak et al., 2012)
Average						21±8	



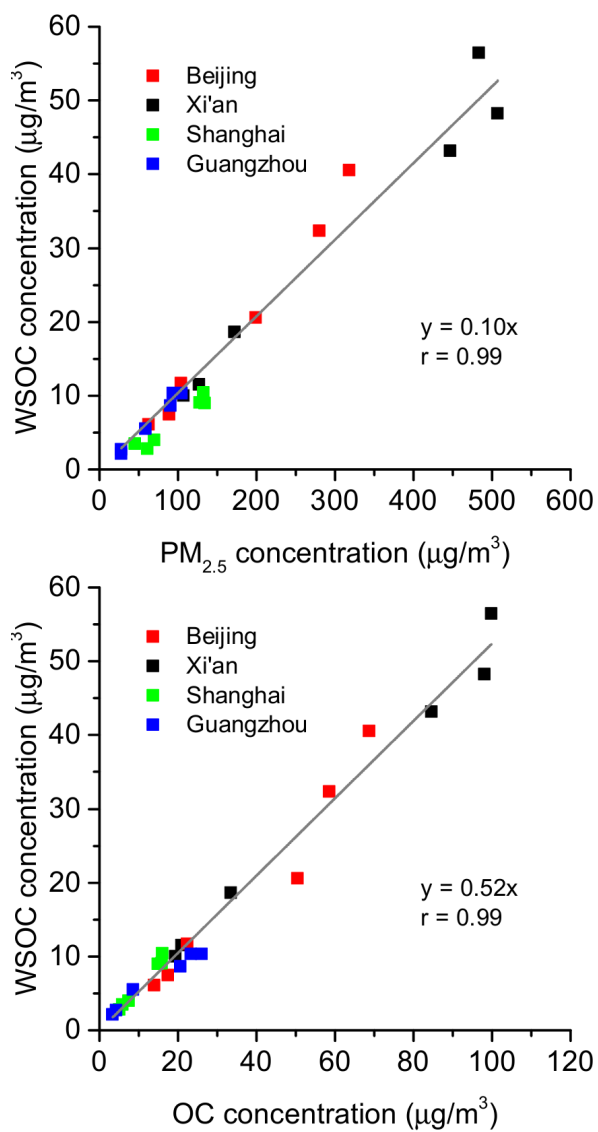
592 **Figure 1.** The AMS²-based source apportionment scheme of WSOC aerosols in this study.
593 See the main text for the equations (i.e., Eq. 4, 5, 9, 10 in the Sec. 2.5) and the offline-AMS &
594 PMF (see the Sec. 2.3).



595



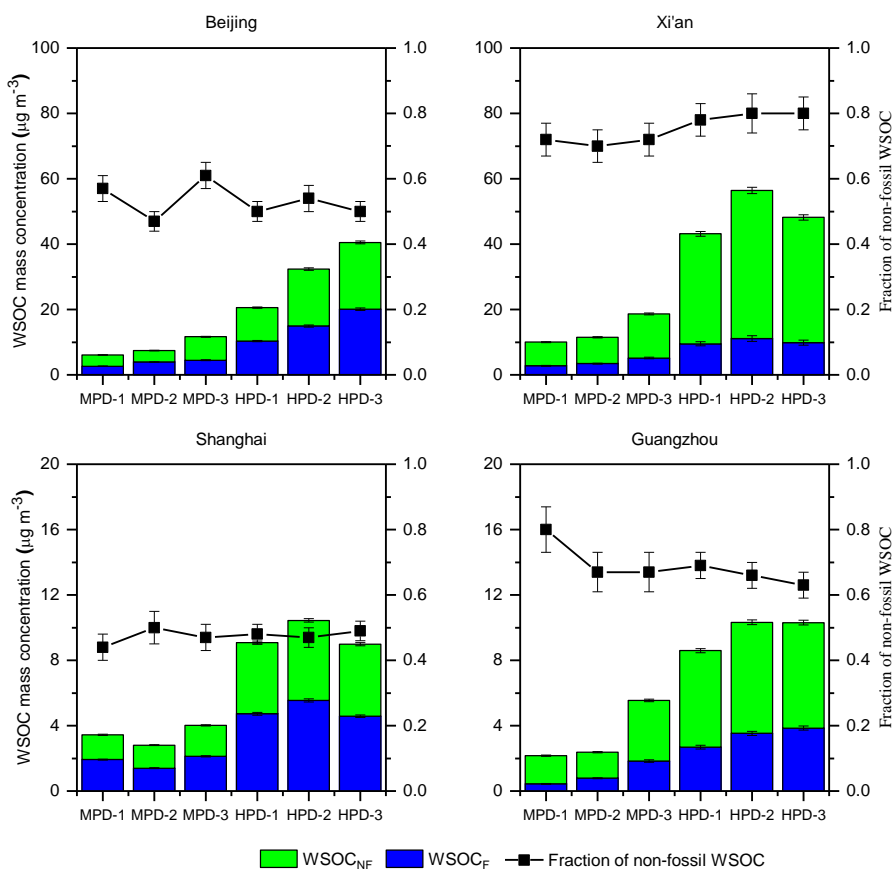
596 **Figure 2.** Linear relationships ($p < 0.01$) of WSOC with $PM_{2.5}$ (top) and OC concentrations
597 (bottom).



598



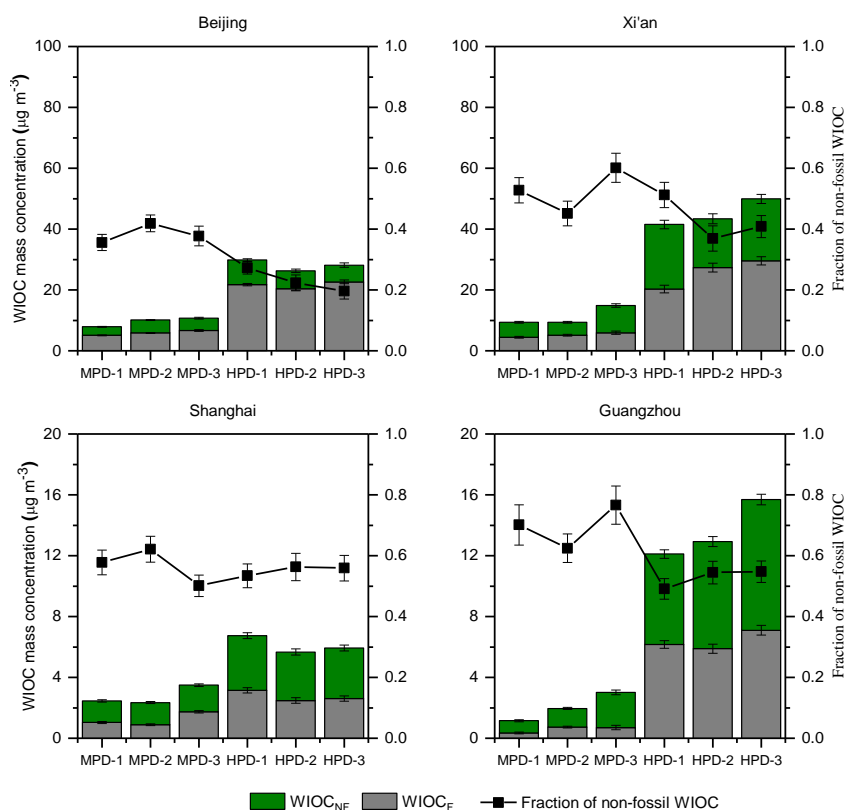
599 **Figure 3.** Mass concentrations ($\mu\text{g}/\text{m}^3$) of WSOC from non-fossil and fossil-fuel sources
 600 (WSOC_{NF} and WSOC_{F} , respectively) as well as non-fossil fractions of the WSOC aerosols from
 601 Beijing, Xi'an, Shanghai and Guangzhou during moderately polluted days (MPD) and heavily
 602 polluted days (HPD). Note the different scaling for different cities.



603



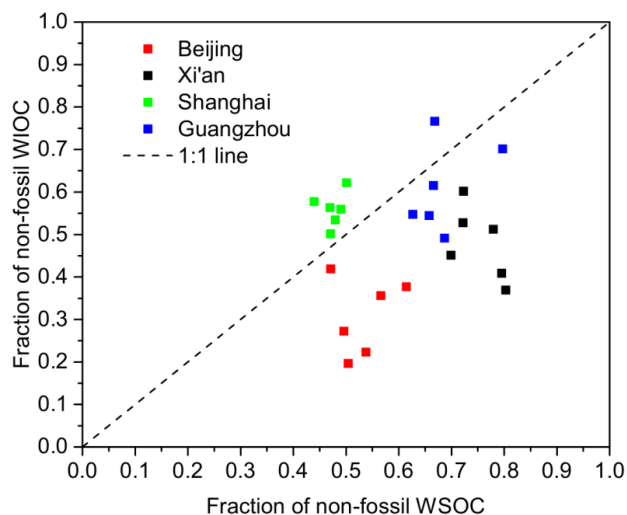
604 **Figure 4.** Mass concentrations ($\mu\text{g}/\text{m}^3$) of WIOC from non-fossil and fossil-fuel sources
605 (WIOC_{NF} and WIOC_F, respectively) as well as non-fossil fractions in the WIOC aerosols from
606 Beijing, Xi'an, Shanghai and Guangzhou during moderately polluted days (MPD) and heavily
607 polluted days (HPD). Note the different scaling for different cities.



608

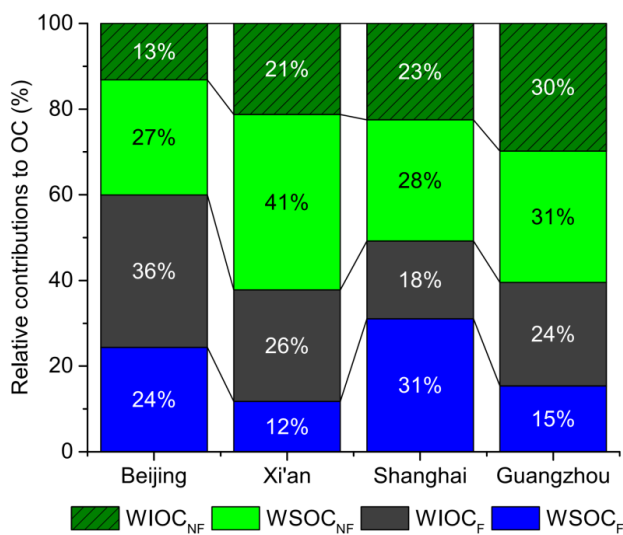


609 **Figure 5.** Relationship between the fraction of non-fossil WIOC and WSOC(a) and averaged
610 relative contribution (%) to OC from WSOC and WIOC from non-fossil and fossil sources
611 (b).



612

613 (a)



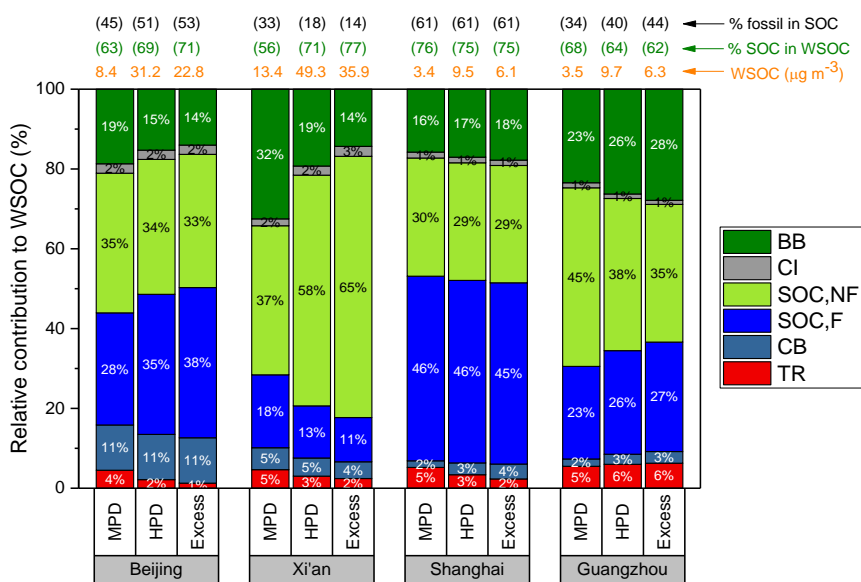
614

615 (b)

616



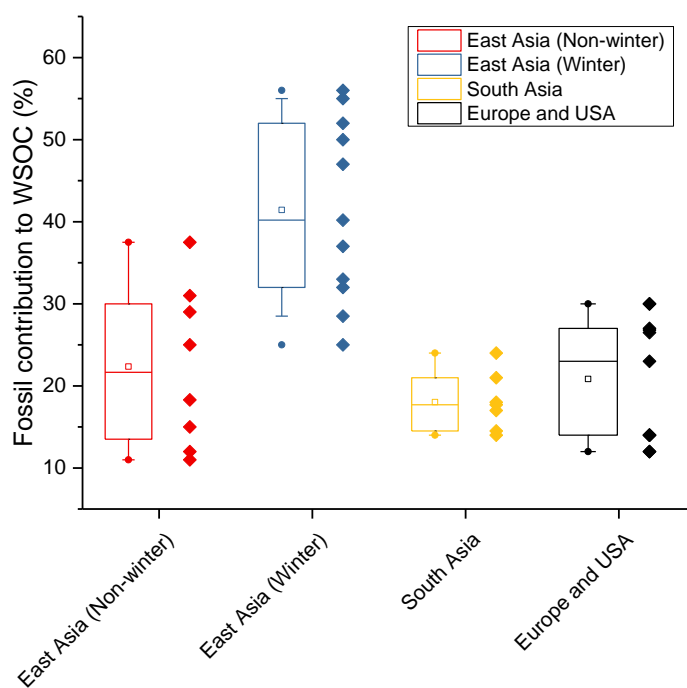
617 **Figure 6.** Relative contributions (%) to WSOC from biomass burning as well as secondary
 618 organic carbon (SOC) from fossil and non-fossil sources ($WSOC_{SOC,F}$ and $WSOC_{SOC,NF}$,
 619 respectively) in different cities during moderately polluted days (MPD) and heavily polluted
 620 days (HPD) as well as their corresponding excess (Excess=HPD-MPD). The numbers above
 621 the bars refer to the average WSOC concentrations and the SOC fractions (%) of WSOC.



622



623 **Figure 7.** Box-plot of the fossil contribution (%) to the WSOC aerosols in East Asia, South
624 Asia, USA and Europe. The box represents the 25th (lower line), 50th (middle line) and 75th (top
625 line) percentiles; the empty square within the box represent the mean values; the end lines of
626 the vertical bars represent the 10th (below the box) and 90th (above the box) percentiles; the
627 solid dots represents the maximum and minimum values; the solid diamonds represent the
628 individual data (Table 1). The data from East Asia is grouped by the winter and non-winter
629 seasons.



630